Supplementary Information: A mathematical model for appressorium–mediated plant infection by the rice blast fungus *Magnaporthe oryzae*

1   Description of the mathematical model

We propose a novel geometric partial differential model for the penetration of the leaf by the rice blast fungus that couples the evolution of the appressorium with a system of reaction–diffusion equations describing the spatiotemporal dynamics of the molecular species. A related model is presented in [8, 13] in which the appressorium geometry is modelled in terms of a bioelastic shell. In this paper the authors show that the basic design of the appressorium is robustly consistent with mechanical principles and has the ability to withstand enormous increases in turgor pressure with apparently little change in shape. However the model considered in [8, 13] is a purely mechanical model of the appressorium geometry and unlike the model we present in this study, it does not consider any aspects of the biochemistry of infection.

In the mathematical setup we consider, the boundary of the appressorium is defined by an evolving closed surface $\Gamma(t)$ and is assumed to lie on an evolving bounded surface $\Upsilon(t)$ that defines the leaf cuticle. For the initial configuration we consider a dome-shaped appressorium with flat face that is in contact with the leaf surface and a hemispherical region above the leaf, see Figure 1 for a schematic representation. This initial setup approximates the geometry of the appressorium 4 hours into a time-course experiment of appressorium development, just before melanin deposition begins.

The evolution laws for the two surfaces take the form of a forced mean curvature flow, see [5] for a mathematical review of such laws, where, in the case of $\Gamma(t)$, the forcing depends on the solution of a system of surface reaction–diffusion

1

equations that hold on $\Gamma(t)$. The system of surface reaction–diffusion equations model the concentration of melanin, the turgor sensor, Septins and F-actin present at the surface of the appressorium. We denote the surface concentrations of these species by u_m, u_{ts}, u_s and u_a, respectively.

We refer to the concentrations of each of the four species in the interior of the appressorium as bulk concentrations and we make the assumption that the diffusion of the bulk concentrations is sufficiently fast such that the bulk concentrations, denoted by B_m, B_{ts}, B_s and B_a, may be treated as spatially uniform. An additional modelling assumption we make is that the total amount, i.e. the combined bulk and surface concentrations, of each species is conserved. We denote these total amounts by T_m, T_{ts}, T_s and T_a with

$$T_i(t) := S_i(t) + B_i(t), \quad \text{for } i = m, ts, s, a \tag{1}$$

where $S_i(t) := \int_{\Gamma(t)} u_i$ gives the total amount of species i on the surface at time t.

Following biological observations, we assume that a key determinant of where species localise in the appressorium is a seeded ring structure, denoted by r. This structure demarcates the appressorium pore to which Septins are initially recruited (see [4]) and where the F-actin network forms during appressorium maturation. Melanin localises only in regions where this seeded structure is absent and is thus recruited to the dome. Melanin is absent from the appressorium pore (see [1]). The core Septins, F-actin and the turgor sensor are all recruited to the seeded ring structure at the appressorium pore.

2   Parameterisation

A description of the parameters used in the model together with their corresponding values is given in Tables 1 and 2. We have attempted, where possible, to use parameter values that have been measured in the experimental literature, [1, 3], or in this study, and in the case that such an estimate is available, the source is provided along with the value in the table. Some of the mechanisms we include, such as the rigidity of the fungus surface depending on Septins and melanin density, are phenomenological in nature, hence, there is no experimental data for the associated parameter values. For such cases, we have simply fitted the values using the model simulations such that the simulated dynamics are qualitatively similar to those observed in experiments. For many of

the parameters involved in the localisation kinetics, we can only determine them up to a multiplicative constant which is given by the total amount of each species present in the appressorium. This is since there is no data on the total amounts of the species we consider, i.e., melanin, Septins, F-actin and the turgor sensor. Due to this uncertainty in some of the parameter values used, in Section 7.2 we report on the results of some basic sensitivity analysis that demonstrates the model possesses a degree of robustness with respect to the parameters.

Table 1: List of parameters used in the evolution laws together with the values used, units and their experimental source (where available).

	Description	Physical Unit
ω_0	fungus rigidity coefficient	$1.92 \times 10^{13} \mathrm{kN}sm^{-3}$ (phenomenological, fitted)
m_1	rigidity magnification due to melanin	1000 Dimensionless (phenomenological, fitted)
m_2	melanin spatial reference value	$1.11 \times T_m \times 10^9 \mathrm{gm}^{-2}$ (fitted, no data on T_m)
s_1	fungus rigidity magnification due to Septins	1000 Dimensionless (phenomenological, fitted)
s_2	reference value of Septins for rigidity	$8.89 \cdot T_s \times 10^8 \mathrm{gm}^{-2}$ (fitted, no data on T_s)
$\bar{t}$	reference time period for turgor generation	$3.6 \times 10^4 \mathrm{s}$ ($4-14$ hpi [11])
P	time pressure coupling constant	$6.94 \times 10^{-2} \mathrm{kNs}^{-1}\mathrm{m}^{-2}$
		(fitted with μ for range ($2 \to 6$ MPa [11])
p_I	pressure at start time	$2 \times 10^3 \mathrm{kNm}^{-2}$ (2MPa) [11]
μ	turgor melanin recruitment coupling	$4 \times (T_m)^{-1} \times 10^3 \mathrm{kNg}^{-1}\mathrm{m}^{-2}$
		(fitted with P to get range, T_m unknown)
a_1	F-actin induced magnification factor	10 Dimensionless
a_2	F-actin spatial reference value	$1.11 \cdot T_a \times 10^9 \mathrm{gm}^{-2}$ (no data on T_a)
d_0	repulsive distance reference value	$7.5 \times 10^{-7} \mathrm{m}$ (regularisation)
r_0	repulsive potential reference value	$3 \times 10^{-2} \mathrm{kNm}^{-1}$ (regularisation)
k	power factor in obstacle potential	12 (regularisation)
σ	fungus surface tension	$3 \times 10^{-3} \mathrm{kNm}^{-1}$
		(≈ 0, regularisation)
σ_l	leaf surface tension	$3 \times 10^4 \mathrm{kNm}^{-1}$ (phenomenological, fitted)
$\bar{H}_l$	threshold value for leaf curvature	$2.67 \times 10^4 \mathrm{m}^{-1}$ (phenomenological, fitted)
ω_l	leaf rigidity coefficient	$1.92 \times 10^{19} \mathrm{kN}sm^{-3}$ (phenomenological, fitted)

3   Geometric evolution laws

In this section, we describe the geometric evolution laws governing the motion of the dome shaped appressorium and the leaf cuticle. We assume each surface may be modelled as a fluidic membrane that resists stretching and bending.
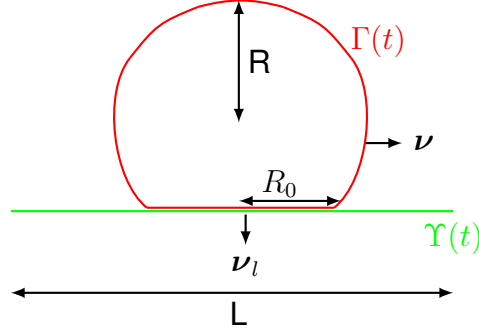
Figure 1: A schematic representation showing the cross-section of the dome-shaped appressorium lying flat on the leaf surface forming a hemispherical region above the leaf.

We denote the outward unit normal, the mean curvature and the normal velocity of $\Gamma(t)$ by $\boldsymbol{\nu}$, H and V respectively and similarly the downward unit normal, the mean curvature and the normal velocity of $\Upsilon(t)$ by $\boldsymbol{\nu}_l$, H_l and V_l. The motion of the appressorium is governed by a geometric evolution law for $\Gamma(t)$ that takes the form of a forced mean curvature flow, see [5], and is formulated as

$$\omega(u_m, u_s)V = p\left(S_m(t), t\right)\left(1 + g_{a_1,a_2}^p(u_a)\right) - \sigma H + g\left(H_l, d(\boldsymbol{x}), d_0, r_0\right) \quad \text{on } \Gamma(t). \quad (2)$$

Next we describe the physical meaning of each of the terms involved in the derivation of the geometric evolution law (2).

(i) The presence of melanin and Septins on the surface of the appressorium are known to contribute to its rigidity, [4], hence where these species are present the resistance to motion, of the surface, is increased. The translation of this biological phenomena into mathematics is obtained via the rigidity function $\omega\left(u_m, u_s\right) := \omega_0(\lambda_{m_1,m_2}(u_m) + \lambda_{s_1,s_2}(u_s))$ where ω_0 is the magnification factor of the rigidity,

$$\lambda_{m_1,m_2}(u_m) := 1 + \frac{m_1}{2}\left(1 + \mathcal{H}^\varepsilon\left(\frac{u_m - m_2}{m_2}\right)\right),$$

and the function $\mathcal{H}^\varepsilon(\alpha) = \tanh\left(\alpha\varepsilon^{-1}\right)$, with $0 < \varepsilon \ll 1$, smoothly approximates the discontinuous step function

$$\mathcal{H}_\alpha := \begin{cases} 1 & \text{if } \alpha \geq 0 \\ -1 & \text{otherwise.} \end{cases}$$

The term $\lambda_{s_1,s_2}(u_s)$ is defined in a similar way with u_m, m_1 and m_2 replaced with u_s, s_1 and s_2 respectively.

(ii) The protrusive force, exerted on the surface of the fungus as a result of the interior turgor pressure, is assumed to be an increasing function of the total amount of melanin recruited to the cell wall layer to reduce the cell porosity and thereby retain solute to generate hydrostatic turgor. Its magnitude is assumed to be increased where F-actin is present on the surface, [4]. Mathematically we model this through the function $p(S_m(t), t)(1 + g^p_{a_1,a_2}(u_a))$, where $p(S_m(t), t)$ models the turgor-generated protrusive force, taking into account the hypothesis that the amount of turgor generated increases as more melanin is recruited to the surface. While $(1 + g^p_{a_1,a_2}(u_a))$ models the magnification, due to F-actin, of this turgor generated protrusive force.

It is observed experimentally, see [2] (Fig.4.(B)) and [11] (Fig.1.), that the turgor pressure exertion by the appressorium during the formation of the penetration hypha roughly increases linearly in time and then becomes constant. We represent these observations mathematically by the function $p_1(t)$ where

$$p_1(t) := \begin{cases} Pt + p_I & \text{if } t < \bar{t}, \\ P\bar{t} + p_I & \text{if } \bar{t} \le t \le T, \end{cases}$$

with p_I denoting the pressure at $t = 0$. Recalling that $S_m(t) = \int_{\Gamma(t)} m$, such that $S_m(t)$ represents the total amount of melanin on the surface of the appressorium, we set

$$p(S_m(t), t) := p_1(t) + \mu S_m(t),$$

where μ is a magnification factor. The presence of F-actin on the surface is mathematically given by $g^p_{a_1,a_2}(u_a)$ and we denote the factor by which its presence magnifies the protrusive force by a_1, resulting in the second function taking the form

$$g^p_{a_1,a_2}(u_a) := \frac{a_1}{2}\left(1 + \mathcal{H}^\varepsilon\left(\frac{u_a - a_2}{a_2}\right)\right).$$

(iii) To model the resistance of the appressorium to stretching we employ the curvature dependent surface tension force $-\sigma H$ which may be thought of mathematically as a regularisation of the evolution law.

(iv) We consider a repulsive force, $r(d(\boldsymbol{x}))$, between the appressorium and the leaf that ceases to exist once the leaf has ruptured. The rupturing of the leaf occurs when the protrusive force defined in (ii) grows large enough to result in the penetration peg significantly deforming the leaf. Mathematically, we

5

model these assumptions via the function

$$g\left(H_l, d(\boldsymbol{x}), d_0, r_0\right) := \begin{cases} 0 & \text{if } \|H_l\|_{L^\infty(\Upsilon(t))} > \bar{H}_l, \\ \boldsymbol{r}(d(\boldsymbol{x}), d_0, r_0) \cdot \boldsymbol{\nu} & \text{otherwise} \end{cases}$$

where the rupture of the leaf cuticle occurs when the maximum value of the mean curvature of the leaf, H_l, exceeds a threshold value $\bar{H}_l$. The repulsive force is modelled by an obstacle potential that prevents the two surfaces intersecting and is given by

$$\boldsymbol{r}(d(\boldsymbol{x}), d_0, r_0) := r_0 k d_0{}^k d(\boldsymbol{x})^{-k-1} \nabla d(\boldsymbol{x})$$

for some large $k \in \mathbb{Z}$, where for $\boldsymbol{x} \in \Gamma(t)$ we define $d(\boldsymbol{x}) := \min_{\boldsymbol{y} \in \Upsilon(t)} |\boldsymbol{x} - \boldsymbol{y}|$ such that $d(\boldsymbol{x})$ is the minimum distance of the point $\boldsymbol{x}$ on the appressorium membrane to the leaf's surface, r_0 is a reference force per unit length associated with the potential and d_0 is some small distance above which the force becomes negligible.

We assume the leaf is deformable and resists penetration and that its motion is governed by a geometric evolution law for $\Upsilon(t)$ which takes the form of a forced mean curvature flow

$$\omega_l V_l = -\sigma_l H_l + g_l(H_l, d_l(\boldsymbol{y}), d_0, r_0) \cdot \boldsymbol{\nu}_l \quad \text{on } \Upsilon(t). \tag{3}$$

Here ω_l is a constant kinetic coefficient, g_l is the interaction force between the leaf and the appressorium akin to g, such that

$$g_l\left(H_l, d(\boldsymbol{x})\right) := \begin{cases} 0 & \text{if } \|H_l\|_{L^\infty(\Upsilon(t))} > \bar{H}_l, \\ -\boldsymbol{r}(d_l(\boldsymbol{y}), d_0, r_0) \cdot \boldsymbol{\nu}_l & \text{otherwise} \end{cases}$$

with $d_l(\boldsymbol{y}) := \min_{\boldsymbol{x} \in \Gamma(t)} |\boldsymbol{x} - \boldsymbol{y}|$ such that $d_l(\boldsymbol{y})$ is the minimum distance of the point $\boldsymbol{y}$ on the leaf's surface to the appressorium membrane. The curvature-dependent surface tension force $-\sigma_l H_l$ models the resistance of the leaf to stretching and again may be thought of mathematically as a regularisation of the evolution law.

Once the leaf has ruptured, i.e. once the maximum value of the mean curvature of the leaf, H_l, exceeds a threshold value $\bar{H}_l$, the leaf dynamics no longer influence the development of the appressorium, hence the geometric evolution law (3) is switched-off and is no longer required.

Our modelling approach in which the surface of the appressorium is treated as a biomembrane that resists stretching has been used in a number of works to

model the deformation of biomembranes of cells and vesicles and is reasonable to describe the deforming pore. In terms of the deformation of the appressorium dome, our model is not justifiable on physical grounds as the physics is largely governed by the properties of the melanised cell wall which we do not explicitly model. As mentioned in the introduction, an alternative mechanical model considered in [8, 13] models the appressorium dome as a bioelastic shell. The model of [8, 13] is valid under the assumption of small deformations and is only capable of describing equilibrium shapes. Moreover, it is not valid in the pore region which is continuously deforming and undergoes large deformations, hence it is not directly applicable in the present study. The constitutive assumptions made on the physics governing the dome in [8, 13] are however not purely phenomenological in nature and arise from rational physically consistent assumptions, making extensions of the model of [8, 13] attractive to describe the deformation of the appressorium dome. An interesting topic for future work would be to consider a hybrid of the two approaches that models the dome of the appressorium as a bioelastic shell and the pore as a fluidic membrane.

4   Surface reaction–diffusion equations

We now define the system of surface reaction–diffusion equations that model the concentrations of melanin, the turgor sensor, Septins and F-actin present on the surface of the appressorium.

We define the material velocity of points on $\Gamma(t)$ by v and the material derivative of a function f with respect to v by $\partial_v^\bullet f := \partial_t f + v \cdot \nabla_\Gamma f$. We note that the material velocity $v = V\nu + v_\tau$ where V is the, previously defined, normal velocity of $\Gamma(t)$ and v_τ is an advective velocity field that is tangential to the surface of the appressorium.

From Fig. 1 A,B in [4] we see the toroidal–shaped F-actin network and the Septins ring assemble colocalise at the appressorium pore. We incorporate these observations into the mathematical model by introducing a function $r(\boldsymbol{x}, t)$ that defines a seeded ring structure at the appressorium pore. At the initial time $t = 0$ we set

$$r(\boldsymbol{x}, 0) := \begin{cases} 0, & \text{if } x_3 > 0, \\ 0, & \text{if } \sqrt{x_1^2 + x_2^2} > R_0, \\ r_1 + r_2\sqrt{x_1^2 + x_2^2}, & \text{otherwise} \end{cases}$$

7

and we assume that $r(\boldsymbol{x}, t)$ does not diffuse around the surface but is simply transported by the motion of the surface such that

$$\partial_{\boldsymbol{v}}^{\bullet} r + r \nabla_\Gamma \cdot \boldsymbol{v} = 0 \quad \text{on } \Gamma(t).$$

Based on biological observations we make the following assumptions as to where on the surface the species localise, see Figure 2:

(i) As melanin is known to reside on the dome of the appressorium we assume it is recruited only to regions on the surface away from the pore, i.e. regions where the seeded ring structure is absent, we denote these regions by $\mathbb{S}_m$ such that

$$\mathbb{S}_m := \{\boldsymbol{x} \in \Gamma(t) | \ r(\boldsymbol{x}, t) = 0\}.$$

(ii) Septins and F-actin localise at the edge of the seeded ring structure, such that

$$\mathbb{S}_s := \{\boldsymbol{x} \in \Gamma(t) | \ r(\boldsymbol{x}, t) > \alpha_s\} \ \text{ and } \ \mathbb{S}_a := \{\boldsymbol{x} \in \Gamma(t) | \ r(\boldsymbol{x}, t) > \alpha_a\}$$

where noting Fig. 1B in [4] we set $\alpha_s > \alpha_a$, since at the centre of the pore the proportion of the concentration of F-actin is greater than the proportion of concentration of Septins. To reflect low levels of recruitment throughout the pore of both Septins and F-actin, we denote the whole pore by

$$\mathbb{S}_r := \{\boldsymbol{x} \in \Gamma(t) | \ r(\boldsymbol{x}, t) > 0\}.$$

(iii) Due to the observed localisation of the Sln1-GFP fusion protein at the appressorium pore we assume the turgor sensor localisation mirrors that of Septins at the appressorium pore, such that

$$\mathbb{S}_{ts} := \{\boldsymbol{x} \in \Gamma(t) | \ r(\boldsymbol{x}, t) > \alpha_{ts}\}$$

with $\alpha_s > \alpha_{ts}$. This assumption is subsequently verified experimentally by the localisation of the Sln1-GFP fusion protein in *M. oryzae*.

To model the surface concentrations of the four species we employ surface reaction–diffusion equations of the form

$$\partial_{\boldsymbol{v}}^{\bullet} u_i + u_i \nabla_\Gamma \cdot \boldsymbol{v} - \nabla_\Gamma \cdot (D_i(u_s) \nabla_\Gamma u_i) = f_i(u_j, B_i, \mathbb{S}_i, T_j) - k_i u_i, \ \text{ for } i = m, ts, s, a, \quad (4)$$

where $j \in \{m, ts, s, a\}$. The third term on the left hand side of (4) models the diffusion of species u_i around the surface of the appressorium. Since Septins act as a diffusion barrier to the other species, [4], we set the effective surface
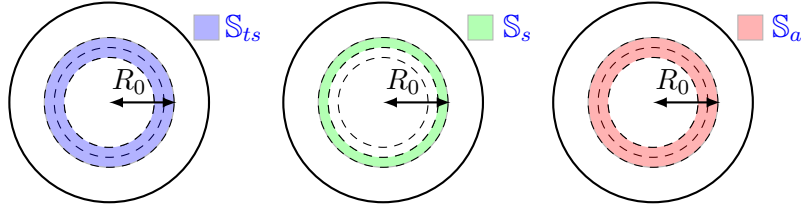
Figure 2: Seeded ring structure in the appressorium pore

diffusivity of melanin, the turgor sensor and F-actin to be very small (and above a given value) on the parts of $\Gamma(t)$ where Septins are present. Mathematically this translates to the Septins dependent diffusion coefficient

$$D_i(u_s) := \begin{cases} d_s & \text{for } i = s, \\ d_i - \frac{d_i q_s}{2}\left(\mathcal{H}^\varepsilon\left(\frac{u_s - s_3}{s_3}\right) + 1\right) & \text{for } i = m, ts, a. \end{cases}$$

The second term on the right hand side of the surface reaction–diffusion equation (4) models a linear degradation of species u_i such that it is reabsorbed into the bulk at a fixed rate k_i, with $k_m = 0$ since no melanin is reabsorbed into the bulk.

The functions $f_i(u_j, B_i, \mathbb{S}_i, T_j)$ model the recruitment of the four species from the interior of the appressorium to its surface. In formulating these functions we assume the following:

 (i) Melanin deposition on the surface is positively correlated with increasing turgor and is inhibited by the amount of turgor sensor present in the bulk at the initial time, [3].

 (ii) Localisation of the turgor sensor is inhibited by the amount of melanin in the bulk at the initial time, moreover this recruitment is assumed to take place only after a certain proportion, q_m, of the bulk melanin has been recruited to the surface, [1]. To this end we define the set $\mathbb{T} := \{t \in (0,T)|\, B_m < q_m T_m\}$.

 (iii) Significant levels of recruitment of Septins from the bulk to a point x on the surface requires the turgor sensor to be present at the point x, with uniform baseline levels of recruitment throughout the pore, [4].

 (iv) Significant levels of recruitment of F-actin from the bulk to a point x on the surface requires Septins to be present at the point x, with uniform baseline levels of recruitment throughout the pore, [4].

The mathematical translation of these assumptions together with the localisa-

tion assumptions of each species lead to the following choices for $f_i(u_j, B_i, \mathbb{S}_i, T_j)$

$$
\begin{aligned}
f_m(B_m, \mathbb{S}_m, T_m, T_{ts}) &:= \Lambda_m \frac{(B_m - q_b \min(T_m, T_{ts}))}{c_m + (B_m - q_b \min(T_m, T_{ts}))}(p(S_m, t) - p_I), \\
f_{ts}(B_{ts}, \mathbb{S}_{ts}, T_m, T_{ts}) &:= \Lambda_{ts}(B_{ts} - q_b \min(T_m, T_{ts}))\chi_{\mathbb{T}}, \\
f_s(u_{ts}, B_s, \mathbb{S}_s) &:= \left(\Lambda_s \chi_{\{u_{ts}>0\}} + \beta_s \chi_{\mathbb{S}_r}\right)B_s, \\
f_a(u_s, B_a, \mathbb{S}_a) &:= \left(\Lambda_a \chi_{\{u_s>0\}} + \beta_a \chi_{\mathbb{S}_r}\right)B_a.
\end{aligned}
$$

Here $q_b \in [0,1]$ denotes the proportion of melanin and turgor sensor that are "bound" and hence unavailable for recruitment to the surface, [1], and $\Lambda_i := l_i \chi_{\mathbb{S}_i}$ with l_i denoting the coefficient of recruitment of species i from the bulk of the appressorium. $\chi_{\mathbb{S}_i}$ denotes the indicator function of the set $\mathbb{S}_i$ such that

$$
\chi_{\mathbb{S}_i}(\boldsymbol{x}) := \left\{ \begin{array}{ll} 1, & \text{if } \boldsymbol{x} \in \mathbb{S}_i, \\ 0, & \text{otherwise} \end{array} \right.
$$

and similarly for $\chi_{\mathbb{T}}(t)$. For the recruitment of melanin we use a Michaelis-Menten formalism. Linear recruitment kinetics alone appear insufficient to model the differences in behaviour between the mutants lacking the turgor sensor and the wild type, i.e., the continual increase of turgor in the mutant versus the maintenance of turgor at a constant level after a certain time in the wild type. This term is interpreted phenomenologically as a means of accounting for the complex melanin biosynthesis pathway, here reduced to a single reaction term, and/or as a simple model for the adsorption of melanin onto the surface. For the remaining species we observe satisfactory results using linear recruitment from the bulk and hence in order to avoid unnecessary complications to the model we adopt linear recruitment kinetics.

The position on the surface at which initial localisation of the different species occurs is guided by a seeded ring structure. Whilst we are interested in understanding why recruitment into an annular region around the pore occurs, this is beyond the scope of the present work and indeed the basic biological mechanisms underlying localisation of the different species are still not fully understood [4]. Note however, our primary modelling hypothesis that the turgor sensor must be present at a point on the surface for subsequent recruitment of Septins and F-actin is not weakened by the inclusion of this ring structure and remains an important aspect of the modelling that is supported by the experimental data.

Regarding the turgor sensor, the interaction we assume between the sensor in the bulk and bulk solute levels (i.e., bulk melanin levels under the modelling simplification) does provide an effective mechanism for turgor sensing due to the positive correlation between melanin deposition in the cell wall, the level

of solute (glycerol) present in the appressorium bulk and turgor generation [3]. There are however, other possible mechanisms by which the sensor could monitor turgor levels, for example through sensing mechanical properties of the appressorium such as wall stress. Further modelling and experimental work is needed to clarify the precise mechanism by which the sensor measures turgor generation.

5 Nondimensionalisation

Denoting scaled dimensionless variables with carets we adopt the following scalings

$$\hat{t} = tt_0{}^{-1}, \; \hat{\boldsymbol{x}} = \boldsymbol{x}x_0{}^{-1}, \; \hat{\boldsymbol{y}} = \boldsymbol{y}x_0{}^{-1},$$

$$\hat{T}_i = T_i T_{i,0}^{-1}, \; \hat{B}_i = B_i T_{i,0}^{-1}, \; \hat{S}_i = S_i T_{i,0}^{-1}, \; \hat{u}_i = x_0^2 u_i T_{i,0}^{-1},$$

$$\hat{m}_2 = \frac{x_0^2 m_2}{T_{m,0}}, \; \hat{s}_2 = \frac{x_0^2 s_2}{T_{s,0}}, \; \hat{a}_2 = \frac{x_0^2 a_2}{T_{a,0}}, \; \hat{s}_3 = \frac{x_0^2 s_3}{T_{s,0}},$$

$$\hat{V} = V t_0 x_0^{-1}, \; \hat{H} = H x_0, \; \hat{V}_l = V_l t_0 x_0^{-1}, \; \hat{H}_l = H_l x_0, \hat{T} = T t_0^{-1}, \; \hat{\bar{t}} = \bar{t} t_0^{-1}$$

$$\hat{d}_0 = \frac{d_0}{x_0}, \; \hat{\sigma} = \sigma (x_0 p_0)^{-1}, \; \hat{\sigma}_l = \sigma_l (x_0 p_0)^{-1}, \; \hat{r}_0 = x_0^{-1} r_0 p_0^{-1}, \; \hat{k}_i = k_i t_0,$$

$$\hat{d}_i = \frac{d_i t_0}{x_0^2}, \; \hat{\omega}_0 = \omega_0 x_0 (p_0 t_0)^{-1}, \; \hat{\omega}_l = \omega_l x_0 (p_0 t_0)^{-1}, \; \hat{\mu} = \mu T_{m,0} p_0^{-1}, \; \hat{l}_{ts,s,a} = l_{ts,s,a} t_0 x_0^2,$$

$$\hat{\beta}_{s,a} = \beta_{s,a} t_0 x_0^2, \; \hat{l}_m = l_m p_0 x_0^2 t_0 T_{m,0}^{-1}, \; \hat{P} = P p_0^{-1} t_0, \; \hat{c}_m = c_m T_{m,0}^{-1}, \; \hat{p}_I = p_I p_0^{-1}, \; \hat{q}_{ts} = T_{ts,0} T_{m,0}^{-1},$$

where we have introduced the characteristic scales for length x_0, time t_0, each species amount $T_{i,0}$, $i = m, s, a, ts$ and pressure p_0. Hence, we denote the scaled appressorium and leaf surfaces as

$$\hat{\Gamma}(t) = \{\hat{\boldsymbol{x}} | x_0 \hat{\boldsymbol{x}} \in \Gamma(t)\} \text{ and } \hat{\Upsilon}(\hat{t}) = \{\hat{\boldsymbol{y}} | x_0 \hat{\boldsymbol{y}} \in \Upsilon(t)\}.$$

Inserting the scalings above into the evolution laws yields the dimensionless forms

$$\hat{\omega}_0 \left(\lambda_{m_1, \hat{m}_2}(\hat{u}_m) + \lambda_{s_1, \hat{s}_2}(\hat{u}_s) \right) \hat{V} = (\hat{p}_1(\hat{t}) + \hat{\mu} \hat{S}_m) \left(1 + g^p_{a_1, a_2}(u_a) \right) - \hat{\sigma} \hat{H}$$
$$+ \hat{g} \left(\hat{H}_l, \hat{d}(\hat{\boldsymbol{x}}), \hat{d}_0, \hat{r}_0 \right) \quad \text{on } \hat{\Gamma}(\hat{t}),$$

and

$$\hat{\omega}_l \hat{V}_l = -\hat{\sigma}_l \hat{H}_l + \hat{g}_l \left(\hat{H}_l, \hat{d}_l(\hat{\boldsymbol{x}}), \hat{d}_0, \hat{r}_0 \right) \quad \text{on } \hat{\Upsilon}(\hat{t}).$$

11

In the above

$$\hat{p}_1(\hat{t}) := \begin{cases} \hat{P}\hat{t} + \hat{p}_I, & \text{if } \hat{t} < \hat{\bar{t}}, \\ \hat{P}\hat{\bar{t}} + \hat{p}_I, & \text{if } \hat{\bar{t}} \le \hat{t} \le \hat{T}, \end{cases}$$

with $\hat{P} = Pp_0^{-1}t_0$, $\hat{p}_I = p_I p_0^{-1}$ and

$$\hat{g}\left(\hat{H}_l, \hat{d}(\hat{\boldsymbol{x}}), \hat{d}_0, \hat{r}_0\right) := \begin{cases} 0, & \text{if } \left\|\hat{H}_l\right\|_{L^\infty(\hat{U}(t))} > \hat{\bar{H}}_l, \\ \boldsymbol{r}(\hat{d}(\hat{\boldsymbol{x}}), \hat{d}_0, \hat{r}_0) \cdot \boldsymbol{\nu}, & \text{otherwise} \end{cases}$$

with $\hat{g}_l$ defined analogously and the obvious notation implied for the distance functions.

For the nondimensionalisation of the reaction–diffusion system, we define the initial condition for the seeded ring structure on the scaled surface via

$$\hat{r}(\hat{\boldsymbol{x}}, 0) = r(x_0\hat{\boldsymbol{x}}, 0) \text{ on } \hat{\Gamma}(0),$$

and the equation it satisfies is

$$\partial_{\hat{\boldsymbol{v}}}^{\bullet}\hat{r} + \hat{r}\nabla_{\hat{\Gamma}} \cdot \hat{\boldsymbol{v}} = 0 \quad \text{on } \hat{\Gamma}(\hat{t}).$$

Hence localisation regions on the scaled surface correspond to

$$\hat{\mathbb{S}}_i := \{\hat{\boldsymbol{x}} \in \hat{\Gamma}(t) | \ \hat{r}(\hat{\boldsymbol{x}}, \hat{t}) > \hat{\alpha}_i\}, \quad \text{for } i = m, ts, s, a,$$

and

$$\hat{\mathbb{T}} := \{\hat{t} \in (0, \hat{T}) | \ \hat{S}_m > q_m\hat{B}_m\}.$$

The dimensionless reaction–diffusion equations thus read

$$\partial_{\hat{\boldsymbol{v}}}^{\bullet}\hat{u}_i + \hat{u}_i\nabla_{\hat{\Gamma}} \cdot \hat{\boldsymbol{v}} - \nabla_{\hat{\Gamma}} \cdot \left(\hat{D}_i(\hat{u}_s)\nabla_{\hat{\Gamma}}\hat{u}_i\right) = \hat{f}_i(\hat{u}_j, \hat{B}_i, \hat{\mathbb{S}}_i, \hat{T}_j) - \hat{k}_i\hat{u}_i, \quad \text{for } i = m, ts, s, a,$$

where $j \in \{m, ts, s, a\}$ and the function

$$\hat{D}_i(\hat{u}_s) := \begin{cases} \hat{d}_s, & \text{for } i = s, \\ \frac{\hat{d}_i}{2}\left(1 - \mathcal{H}^\varepsilon\left(\frac{\hat{u}_s - \hat{s}_3}{\hat{s}_3}\right)\right), & \text{for } i = m, ts, a, \end{cases}$$

and the localisation functions are given by

$$\hat{f}_m(\hat{B}_m, \hat{\mathbb{S}}_m, \hat{T}_m, \hat{T}_{ts}) := \hat{l}_m\chi_{\hat{\mathbb{S}}_m}\frac{\left(\hat{B}_m - q_b\min(\hat{T}_m, q_{ts}\hat{T}_{ts})\right)}{\hat{c}_m + \left(\hat{B}_m - q_b\min(\hat{T}_m, q_{ts}\hat{T}_{ts})\right)}((\hat{p}_1(\hat{t}) + \hat{\mu}\hat{S}_m) - \hat{p}_I),$$

$$\hat{f}_{ts}(\hat{B}_{ts}, \hat{\mathbb{S}}_{ts}, \hat{T}_m, \hat{T}_{ts}) := \hat{l}_{ts}\chi_{\hat{\mathbb{S}}_{ts}}\chi_{\hat{\mathbb{T}}}(\hat{B}_{ts} - q_b\min(q_{ts}^{-1}\hat{T}_m, \hat{T}_{ts}))$$

$$\hat{f}_s(\hat{u}_{ts}, \hat{B}_s, \hat{\mathbb{S}}_s) := \left(\hat{l}_s\chi_{\hat{\mathbb{S}}_s}\chi_{\{\hat{u}_{ts}>0\}} + \hat{\beta}_s\chi_{\hat{\mathbb{S}}_r}\right)\hat{B}_s,$$

$$\hat{f}_a(\hat{u}_s, \hat{B}_a, \hat{\mathbb{S}}_a) := \left(\hat{l}_a\chi_{\hat{\mathbb{S}}_a}\chi_{\{\hat{u}_s>0\}} + \hat{\beta}_a\chi_{\hat{\mathbb{S}}_r}\right)\hat{B}_a.$$

6 Numerical approximation

The equations described above result in a complex highly coupled system of equations in which coupled nonlinear geometric evolution laws are in turn coupled to semi-linear systems of reaction–diffusion equations, posed on evolving surfaces. For such systems, analytical solutions are in general unavailable and one must resort to numerical simulations to understand the behaviour of the solution. The numerical method we implement to solve these coupled systems follows that described in [7], in which the evolving surface finite element method, see [6], is employed for the approximation of the surface reaction–diffusion equations together with a finite element approximation of a parametric reformulation of the evolution laws, see [5]. We will report on a detailed description of the resulting discretisation elsewhere and hence we do not present further details here.

7 Simulations

To simplify the coefficients in the dimensionless system we make the choice $x_0 = 1.5 \times 10^{-5}\mathrm{m}$, time $t_0 = 1.44 \times 10^5\mathrm{s}$, and pressure $p_0 = 2\mathrm{MPa}$. In all the simulations the initial conditions are set to be a flat, square leaf surface, with length $L = 1$, and the appressorium is taken to be partially spherical with the dome corresponding to a portion of a sphere of radius $R = 0.2$ with a flattened pore, of diameter $2R_0 = 0.176$. The initial values for all the species (melanin, Septins, F-actin and the turgor sensor) are such that in the wild type, the total amount of each species is equal to one with each species only present in the bulk, whilst in the mutant cases the total amount of the turgor sensor is set to zero with all other initial amounts unchanged. The parameter values that were used in each of the simulations are given in Table 3, where we have dropped the carets for ease of notation.

7.1 Results

We report on the simulations in the attached movies and figures. The movies Extended Material Movie 1 and Extended Material Movie 2 show the dynamics of the infection process in the wild type fungus and the mutant lacking the turgor sensor respectively. Fig. 2a and Fig. 2b show the position of the fungus at the end-time of the simulations (0.5 in dimensionless time corresponding to a time of

13

24 hours post infection), where we have removed the leaf cuticle from the top left panel of the figures in order to show the base of the appressorium. Fig. 2a and Fig. 2b show the evolution of the turgor pressure and the maximum curvature of the leaf against time for both cases. We observe successful penetration of the cuticle only in the wild type case whilst the threshold curvature value is never reached in the mutant lacking the turgor sensor. The observed localisation of the species is consistent with the experimental data in both position and time scale. Initially, melanisation of the dome occurs in both cases and subsequently in the wild type case, the turgor sensor, Septins and F-actin are all recruited to the pore whilst in the mutant no localisation of any species other than melanin occurs on the surface. In the wild type simulations a penetration peg forms around $t = 0.32$ (corresponding to 16.8 hours post infection) and this causes large curvatures to develop in the leaf surface causing it to rapidly rupture. With only the low levels of uniform recruitment of Septins and F-actin to the pore, the peg is not formed in the mutant lacking the turgor sensor, despite the fact that overall it generates a larger turgor pressure (due to the increased amount of melanin deposited on the surface). In the mutant, the protrusive force is not localised by F-actin and the mutant does not puncture the leaf.

7.2 Robustness Analysis

Since we have a large number of parameters in the model and only some of them come from experimental estimates, we conducted a rudimentary sensitivity analysis consisting of extra simulations in which we increased and decreased each of the parameters individually (i.e., one by one) by 10% of their magnitude. In all cases the qualitative features of the simulations remained unchanged with penetration and normal polarisation occurring in the wild type case and no penetration and no Septins and F-actin localisation in the mutant lacking the turgor sensor.

References

[1] Bourett, T. M., Howard, R. J. *In vitro* development of penetration structures in the rice blast fungus *Magnaporthe grisea*. *Can J Bot* **68**, 329–342 (1990).

[2] Bechinger, C., Giebel, K.-F. , Schnell, M., Leiderer, P., Deising, H. B., Bastmeyer, M. Optical measurements of invasive forces exerted by appressoria of a plant pathogenic fungus. *Science* **285**, 1896–1899 (1999).

[3] Chumley, F. G., Valent, B. Genetic-Analysis of Melanin-Deficient, Non-pathogenic Mutants of *Magnaporthe grisea*. *Mol Plant Microbe In* **3**, 135–143 (1990).

[4] Dagdas, Y. F., Yoshino, K., Dagdas, G., Ryder, L. S., Bielska, E., Steinberg, G., Talbot, N. J. Septin-mediated plant cell invasion by the rice blast fungus, *Magnaporthe oryzae*. *Science* **336**, 1590–1595 (2012).

[5] Deckelnick, K., Dziuk, G., Elliott, C. M. Computation of geometric partial differential equations and mean curvature flow. *Acta Numer* **14**,139-232 (2005).

[6] Dziuk, G., Elliott, C. M. Finite element methods for surface PDEs. *Acta Numer* **22**, 289–396, (2013).

[7] Elliott, C. M. , Stinner, B., Venkataraman, C. Modelling cell motility and chemotaxis with evolving surface finite elements. *J R Soc Interface* **9**, 3027–3044 (2012).

[8] Goriely, A., Tabor, M. Estimates of biomechanical forces in *Magnaporthe grisea*. *Myc Res* **110**, 755–759 (2006).

[9] García-Peñarrubia, P., Gálvez, J. J., Gálvez, J. Mathematical modelling and computational study of two–dimensional and three–dimensional dynamics of receptor–ligand interactions in signalling response mechanisms. *J Math Biol* **69**, 1–30 (2013).

[10] Hamer, J. E., Howard, R. J., Chumley, F. G., Valent, B. A Mechanism for Surface Attachment in Spores of a Plant Pathogenic Fungus. *Science* **239**, 288–290 (1988).

[11] Howard, R. J., Ferrari, M. A., Roach, D. H., Money, N. P. Penetration of hard substrates by a fungus employing enormous turgor pressures. *Proc Natl Acad Sci USA* **88**, 11281–11284 (1991).

[12] Linderman, J. J., Lauffenburger, D. A. Analysis of intracellular receptor/ligand sorting. Calculation of mean surface and bulk diffusion times within a sphere. *Biophys J* **2**, 295–305 (1986).

[13] Tongen, A., Goriely, A., Tabor, M. Biomechanical model for appressorial design in *Magnaporthe grisea*. *J Theor Biol* **240**, 1–8 (2006).

[14] Wilson, R. A., Talbot, N. J. Under pressure: investigating the biology of plant infection by *Magnaporthe oryzae*. *Nat Rev Microbiol* **7**, 185–195 (2009).

Table 2: List of parameters used in the surface reaction–diffusion equations together with the values used, units and their related experimental estimates (when available otherwise fitted).

	Description	Physical Unit
R_0	radius of the ring structure (pore at 4 hpi)	$1.32 \times 10^{-6}\mathrm{m}$ [11]
R	initial radius of the appressorium	$3 \times 10^{-6}\mathrm{m}$ [11]
r_1	reference value for initial ring structure	0.33 (Dimensionless)
r_2	reference value for initial ring structure	$1.02 \times 10^{-4}\mathrm{m}^{-1}$ (phenomenological)
d_m	diffusion coefficient of melanin	$0\mathrm{m}^2\,\mathrm{s}^{-1}$
d_{ts}	diffusion coefficient of the turgor sensor	$1.6 \times 10^{-15}\,\mathrm{m}^2\,\mathrm{s}^{-1}$
d_a	diffusion coefficient of F-actin	$1.6 \times 10^{-15}\,\mathrm{m}^2\,\mathrm{s}^{-1}$
		c.f., [9] and [12]
		for receptor-complex diffusion
d_s	diffusion coefficient of Septins	$1.6 \times 10^{-18}\,\mathrm{m}^2\,\mathrm{s}^{-1}$
		(Smaller to fit absence from pore)
s_3	reference value for Septins mediated diffusion	$4.44 \cdot T_s \times 10^8 g\mathrm{m}^{-2}$ (no data, T_s unknown)
q_s	proportion diffusivity reduction by Septins	0.999 Dimensionless
k_m	degradation rate of melanin	$0\mathrm{s}^{-1}$
k_{ts}	degradation rate of the turgor sensor	$6.9 \times 10^{-7}\mathrm{s}^{-1}$
k_s	degradation rate of Septins	$6.9 \times 10^{-7}\mathrm{s}^{-1}$
k_a	degradation rate of F-actin	$6.9 \times 10^{-7}\mathrm{s}^{-1}$
		3 values above fitted
		to localisation timescales
l_m	recruitment coefficient of melanin	$4.63 \times T_m \times 10^2 \mathrm{gs}^{-1}\mathrm{kN}^{-1}$ (fitted to
		saturation in in wild type, T_m unknown)
		and continuous recruitment in mutant)
l_{ts}	recruitment coefficient of the turgor sensor	$3.09 \times 10^4\mathrm{m}^{-2}s^{-1}$
		(fitted to localisation time)
l_s	recruitment coefficient of Septins	$3.09 \times 10^4\mathrm{m}^{-2}s^{-1}$
		(fitted to localisation time)
l_a	recruitment coefficient of F-actin	$3.09 \times 10^7\mathrm{m}^{-2}s^{-1}$
		(fitted to localisation time)
β_s	uniform recruitment coefficient of Septins	$3.09 \times 10^3\mathrm{m}^{-2}s^{-1}$
		(fitted to match desired profile)
β_a	uniform recruitment coefficient of F-actin	$3.09 \times 10^3\mathrm{m}^{-2}s^{-1}$
		(fitted to match desired profile)
c_m	saturation level of melanin recruitment	$10 \times T_m g$ (fitted to match desired profiles)
α_{ts}	coefficient determining turgor sensor localisation	0.3 Dimensionless
α_s	coefficient determining Septins localisation	0.6 Dimensionless
α_a	coefficient determining F-actin localisation	0.3 Dimensionless
q_b	fraction of 'bound' bulk melanin and turgor sensor	0.55 Dimensionless
q_m	fraction of melanin for turgor sensor recruitment	0.95 Dimensionless

Table 3: Dimensionless parameter values used in the simulations.

ω_0	m_1	m_2	s_1	s_2	$\bar{t}$	P	p_I	μ
1	1×10^3	0.25	1×10^3	0.2	0.25	5	1	2

a_1	a_2	σ	σ_l	$\bar{H}_l$	k	ω_l	r_1	r_2
5	0.25	0.1	1×10^6	0.4	12	1×10^6	0.33	6.66

d_m	d_{ts}, d_a	d_s	s_3	q_s	k_m	k_{ts}, k_s, k_a	l_m	c_m
0	1×10^{-2}	1×10^{-5}	0.1	0.999	0	0.1	30	10

l_{ts}, l_s, l_a	β_s, β_a	α_{ts}	α_s	α_a	q_b	q_m	d_0	r_0
1	0.1	0.3	0.6	0.3	0.55	0.95	0.05	1